



## Full Length Article

## Morphometry, bathymetry, gravity analyses and active tectonics of the petroliferous Gulf of Mannar in the Indian sector

Kutubuddin Ansari <sup>a</sup>, Mery Biswas <sup>b</sup>, Adrija Raha <sup>b</sup>, M.L. Shilpashree <sup>c</sup>, Soumyajit Mukherjee <sup>d,\*</sup>

<sup>a</sup> Integrated Geoinformation (IntGeo) Solution Private Limited, New Delhi, 110 025, India

<sup>b</sup> Department of Geography, Presidency University, 86/1 College Street, Kolkata, 700 073, West Bengal, India

<sup>c</sup> Department of Petroleum Engineering and Earth Sciences, UPES Dehradun, Energy Acres, UPES, Bidholi, Via, Prem Nagar, Uttarakhand 248 007, India

<sup>d</sup> Department of Earth Sciences, Indian Institute of Technology Bombay, Powai, Mumbai 400 076, Maharashtra, India

## ARTICLE INFO

## Article history:

Received 27 August 2024

Received in revised form

20 March 2025

Accepted 21 March 2025

Available online xxx

## Keywords:

Tectonics

Gravity analysis

Indian plate

Morphometric analyses

Basin tectonics

Active tectonics

## ABSTRACT

The Gulf of Mannar has been producing natural gas in the Sri Lankan portion. This indicates that a detail geoscientific study is to be undertaken from the Indian section of the gulf, which can have a far-reaching implication in the Indian petroleum geoscience. In this work, morphometric and gravity studies were made from the gulf/basin near the onshore area, and bathymetric studies from the offshore portion of the Mannar basin within the Indian sector. Five watersheds were delineated based on study of eight geomorphic parameters on remote sensing images from the onshore area. Out of these watersheds 4 and 5 are found to be presently tectonically most active. Well-bore stability issue is to be considered while drilling these portions in future. We further prepared a regional contour map for the offshore study area, analysed the free air gravity data from the onshore area, and deduced the First Vertical Derivative (FVD) and Tilt Derivative Ratio (TDR). Bathymetric height gradually increases along the north-south trend from the coast region of the study area towards the central region, while the gravity magnitudes display a very sharp gradient (around 150 mGal). The gravity anomaly shows positive values at continental shelf (0–160 mGal), which includes parts of watersheds 1 and 3 and attains negative magnitude (up to –20 mGal) towards the basin area. Negative gravity anomaly in the offshore area may indicate presence of hydrocarbon but more studies are needed for confirmation. Apparently, almost a negative correlation (except watershed 1) between surface elevation and free air gravity magnitudes has been found.

© 2025 The Authors. Publishing services provided by Elsevier B.V. on behalf of KeAi Communication Co. Ltd. This is an open access article under the CC BY-NC-ND license (<http://creativecommons.org/licenses/by-nc-nd/4.0/>).

## 1. Introduction

Climatic conditions shape the features on Earth while tectonic stresses deform the lithosphere. Disturbance in these processes result in shifting the state from dynamic equilibrium to a disequilibrium state (Mathew et al., 2016). Signatures of disequilibrium affect the river morphology (Biswas et al., 2022a). A watershed is a land that drains water obtained from natural sources such as rain and snowmelt. Longitudinal profile, hypsometric integral and curve, and asymmetry factor are studied customarily to understand

the influence of tectonics and the behaviour of watersheds/basins. Digital representations of topography have been used increasingly to calculate morphometric parameters, such as through the Digital Elevation Models (DEMs).

The Indian plate is tilted towards east (Radhakrishna, 1993). Most of the drainages in India therefore flow towards east. The failed rifts and Gondwana basin along the east coast developed coevally as the Gondwana supercontinent rifted (Collins and Pisarevsky, 2005; Twinkle et al., 2016). The tectonics of the Mannar Basin is complex and dates back to the rifting of the Gondwanaland (e.g., Herath et al., 2017) (Fig. 1). The evolution of the Indian east coast has been explained by many (e.g., Lal et al., 2009). However, morphometric properties over spatial and linear-scales (e.g., Aiken and Brierley, 2013; Anand and Pradhan, 2019; Fraefel, 2008; Różycka and Migoń, 2021) have not been carried out from the watershed areas that drain into the Mannar basin.

\* Corresponding author.

E-mail addresses: [smukherjee@iitb.ac.in](mailto:smukherjee@iitb.ac.in), [soumyajitm@gmail.com](mailto:soumyajitm@gmail.com)  
(S. Mukherjee).

Peer review under the responsibility of Editorial Office of Petroleum Research.

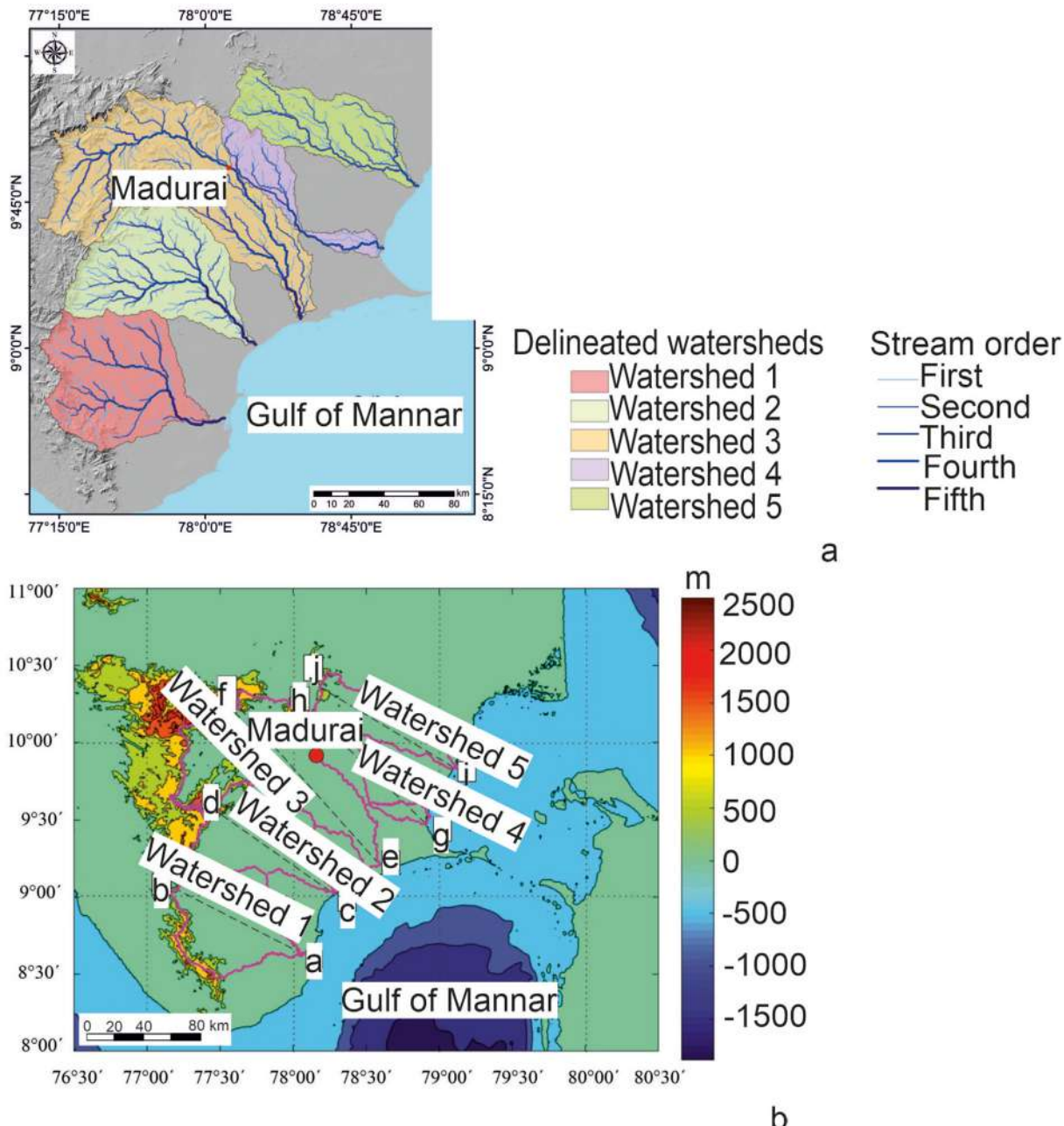


**Fig. 1.** (a) Left- Study area with watersheds overlaid on the hillshade map. Right – India map ([https://www.mapsofindia.com/lat\\_long/](https://www.mapsofindia.com/lat_long/)). (b) Shaded relief contour map plotted from GEBCO bathymetry data over the Indian SE continental margin, which include Gulf of Mannar. Positive magnitudes indicate elevation in m. Negative measurements connote the bathymetric depth below the mean sea level.

In the southern part of the Indian continent, near the Trivandrum Block (Plavsa et al., 2014) and the southern Madurai block (Plavsa et al., 2014), the basement rocks are metasedimentary protoliths of felsic rocks and anorthosites. NE–SW trending rift-related horst-graben structural features occur in the Madurai–Rameswaram cut (Prabhakar and Zutshi, 1993).

This work aims to study onshore and offshore tectonics of the Mannar basin in the Indian portion. We perform morphometry on the rivers in the five watersheds in the Trivandrum Block using remote sensing images. Researches on slope-area relationships in intraplate with special emphasis on clustering of morphotectonic indicators (e.g., Biswas et al., 2023a, b) are not too many. Previous workers did perform/compile different

geomorphologic studies in and around the study area (e.g., Reshma et al., 2021, 2022; Sivakumar, 2016; Thanikachalam and Ramachandran, 2002). However, these authors did not apply any statistical techniques such as clustering to assess the active tectonic prioritization amongst the watersheds. To establish connection with the morphometry in the regional area, bathymetry and gravity anomalies variation are also studied in this work. We delineate lineaments from the land (watershed) areas that hint the tectonics. The sedimentary architecture of the basin can be worked out from the bathymetric studies of basins (Dmitrieva et al., 2018). On the other hand, gravity studies from basis can indicate deep faults, isostatic anomalies etc (Zhang et al., 2019).

## 2. Study area

The Gulf of Mannar/Mannar Basin, is located between the southeast coast of India and the western margins of the island country Sri Lanka. The gulf covers ~45,000 km<sup>2</sup>. Rivers belonging to five different watersheds drain into the basin. These rivers originate from the Western Ghat (Cardamom hill massif) and flow eastwards into the Gulf of Mannar. Rivers of the watersheds 1 and 4 are perennial (Fig. 1a). The offshore study area is delimited at west by the south Indian peninsula, at north by the Palk Strait and at east by the Indo-Lanka Maritime Boundary (Fig. 2).

## 3. Relevance in hydrocarbon geosciences

The Mannar basin has been classified as a Category II basin within a rifted setting, and also as a type II<sub>B</sub>: pericratonic rift (Dwivedi, 2016; Ratheesh Kumar et al., 2020). North to the onland part of the study area is the Ramnad sub-basin, which is a proven hydrocarbon province (Kularathna et al., 2020; Vasudevan et al., 2008). Interestingly, from the Sri Lankan portion of the Mannar basin, gas discoveries have been made (Kularathna et al., 2020). Eight hydrocarbon blocks were discovered in 2011 from the Sri Lankan Mannar Basin that can have >2 trillion cubic feet of natural gas (Kularathna et al., 2020; Narasaiah, 2017). As per the United States Geological Survey's (USGS's) estimate, a prodigious proportion of oil and gas exist in the Mannar basin (as referred in Piyadasa (2014)).

Thickness of sediments in Mannar basin can be within ~2–6 km. These sediments range in age from Late Jurassic up to Recent (Ratheesh-Kumar et al., 2020). The Indian part of the Mannar basin, on the other hand, consists of three major stratigraphic sequences, five play types, and Type II and II kerogens (review in Singh and Rao (2021)). Gas shows were documented by seismic studies by Das et al. (2008) from the Indian part of the Mannar basin. Recently, Mishra et al. (2021) through seismic studies inferred gas hydrate deposits (gas chimneys and pull-down structures) from the Mannar basin from the Indian portion. Commercial production from Mannar basin has not yet started from the Indian side.

Geoscientific information from this basin in the Indian part is still scanty, and till 2008, only six wells have been drilled (Das et al., 2008). Therefore, a detail geoscientific study from the Indian portion of the Mannar and the adjoining areas is important from the exploration perspective.

## 4. Geology & geophysics

The high-grade massifs of the Neoarchean emplacement history and Early Paleoproterozoic metamorphic history have been retained in the arc magmatic rocks that predominate in the Nilgiri, Salem, Madras and other crustal blocks (e.g., Clark et al., 2009; Praveen et al., 2013; Santosh et al., 2013; Brandt et al., 2014; Samuel et al., 2014). The Mannar Basin was affected by several regional tectonic events such as rifting, sea-floor spreading, volcanic activities, continental collision and subduction (Ratnayake et al., 2014). During the Middle Jurassic, the rifted Mannar basin began to evolve when the eastern Gondwanaland separated from the western part. A second rifting between the Greater India and the Antarctica-Australia followed took place prior to ~134 Ma (Ali and Aitchison, 2008; Dasgupta, 2019; Desa et al., 2006; M.V. Ramana et al., 1994a, 1994b, 2001). During the Cretaceous, Greater India underwent consecutive breakups, such as the separation of Madagascar (~90 Ma) and then Seychelles (~65 Ma). These processes were analogous to events of basalt flows (Chatterjee et al., 2013; Storey et al., 1995).

There are seven dominant geologic formations within South Madurai Block (SMB) and Trivandrum Block (TB). The western part near the catchment of the watersheds belongs to the Northern Madurai Block (NMB) (Fig. 2). Based on geochronology (Ghosh, 2004; Mohan et al., 2013), an Early Neoproterozoic (ca. 730–700 Ma) thermal event presumably weakened the southern Salem block.

Marine bathymetry survey revealed coast-parallel ridges and few depressions in the shallow portion of the Indian Mannar basin (Satyanarayana et al., 2016). Lithospheric extension with amplitude  $\beta = 1.15\text{--}1.25$  has been deduced from the Sri Lankan portion of the Mannar basin during the basin's second rifting stage in the Late Cretaceous (Galushkin and Dubinin, 2020). Moho depth below the Mannar basin ranges ~16–36 km below the mean sea level. Mannar basin's crustal structure is comparable with the Indian subcontinent (Kumar et al. 2009a, 2009b).

## 5. Data acquisition & method

### 5.1. Morphometric studies

Shuttle Radar Topography Mission (SRTM) – Digital Elevation Model (DEM) of 30 m resolution were downloaded from the United States Geological Survey (USGS) Earth Explorer. The software ArcGIS 10.4 was used to extract the geomorphic indices and morphometric properties from the DEM data. Twelve SRTM DEM tiles were mosaiced and streams were delineated, and then the watersheds were demarcated. Drainages were demarcated from the Digital Elevation Model (DEM). The SRTM and the DEM were captured on 11-Feb-2000 and released on 23-Sept-2014. Being cloud-free, atmospheric corrections were not required on the photos. Various areal, relief and linear features are assessed using the ArcGIS version 10.3 (2018). The D8 Python tool built into ARC GIS was used to create and extract the stream network using the specified threshold value. Each pixel's eight neighbors' pixels have been used to determine the slope direction.

According to Strahler (1952), hypsometric curve (HC) represents the area distribution within a basin with respect to altitude. The topography of the basin is described by HC (Pérez-Peña et al., 2009). It can be used to clarify how tectonics, geomorphic processes and basin topography are inter-related (Štěpančíková et al., 2008). The percentage technique was used to analyze HCs (Strahler, 1952; Anand and Pradhan, 2019; Biswas et al., 2022a, 2022b). The HC is produced by plotting the relative area ( $a/A$ ) on the ordinate (y-axis) and the relative elevation ( $h/H$ ) on the abscissa (x-axis).

Geomorphic/river systems are significantly impacted by recent tectonic activity. Long profiles show where the slope breaks and where knick points emerge as a result of tectonics and lithology from source to mouth. Long profile denotes the break of slope and formation of knick points due to tectonics and lithology from source to mouth (Dasgupta et al., 2022; Biswas et al., 2022a, 2022b).

The linear and the logarithmic functions are:

$$y = ax + b \quad (\text{eqn 1})$$

$$y = a \ln x + b \quad (\text{eqn 2})$$

Here  $y$ : elevation ( $H/H_0$ ;  $H$ : elevation of each point,  $H_0$ : elevation at the source),  $x$ : length of the river ( $L/L_0$ ;  $L$ : distance of the point from the source,  $L_0$ : total length of the stream) and  $a$ ,  $b$ : coefficients derived independently from each profile (Table 1). The best fit is determined using the correlation coefficient ( $R$ ). The best-fitting curve is the one with the highest  $R^2$  magnitude.

In this study, few aerial and linear parameters have been used to assess the recent tectonics of the study area. A longitudinal profile

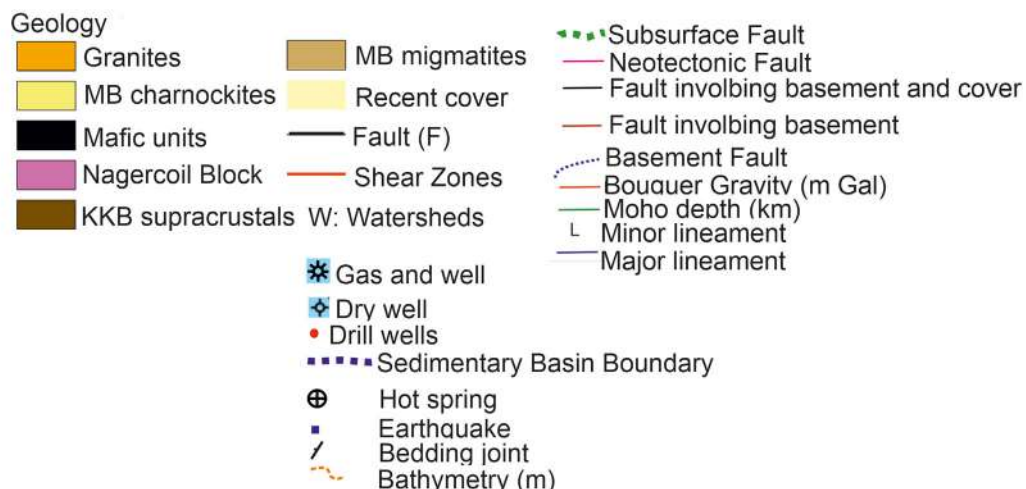
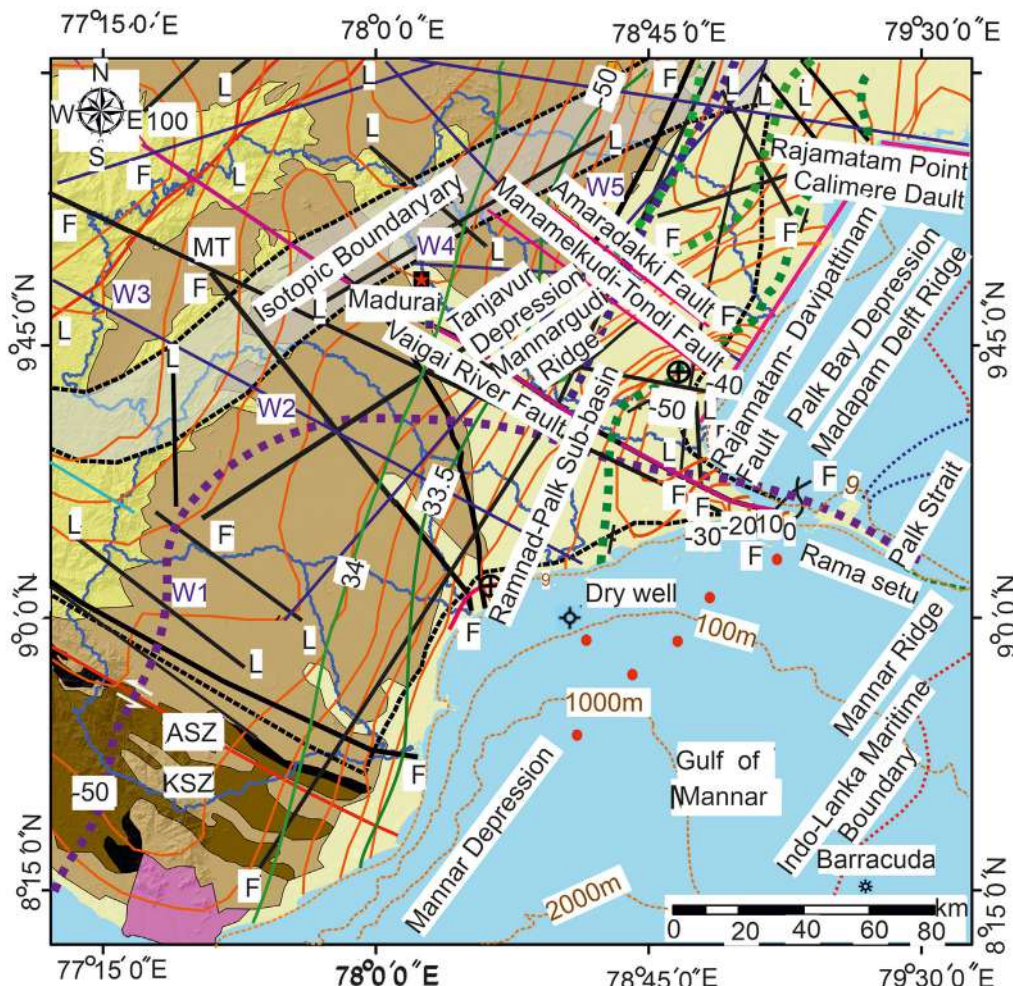


**Fig. 2.** Map showing the faults, lineaments and shear zones. ASZ: Achankovil Shear Zone, KKB: Kerala Khondalite Belt, MB: Madurai Block, MT: Madurai Terrain, NMB: Northern Madurai Block, SMB: South Madurai Block, TB: Trivandrum Block (Shaji et al., 2014), KSZ: Kanyakumari Shear Zone (Gopalakrishnan, 2003). W1, W2 etc.: Watersheds. NW–SE and SE–SW aligned faults, isotopic boundary and Bouguer anomalies (mGal) presented. Compiled from Chari et al. (1995), Gopalakrishnan (2003), Harinarayana et al. (2003), Mahadevan (2003), Reddy et al. (2003), Das et al. (2008), Premaratne et al. (2013), Shaji et al. (2014), Premaratne (2015a, 2015b), Satyanarayana et al. (2016), Twinkle et al. (2016), Herath et al. (2017), Dasgupta (2019), Dasgupta et al. (2000), Galushkin and Dubinin (2010), Kularatna et al. (2020), Premaratne and Ranaweera (2021), Dasgupta et al. (2022). Pedro-1, Delft-1, Palk Bay-1, Pasalai-1 2&3, Pearl-1 (Premaratne et al., 2013), Karaikal High, Portnov High (Satyanarayana et al., 2016), and Dorado and Dorado North (Premaratne and Ranaweera, 2021) are other important structures/drill locations related to the Mannar basin but those fall outside the map.

**Table 1**

Calculated  $R^2$  values from linear, exponential, logarithmic and power curves for five watersheds. Red fonts: Highest magnitudes of  $R^2$  values calculated in different ways for the watersheds.

Master stream of Watersheds	$R^2$ (unitless)			
	Linear	Exponential	Logarithmic	Power
1	0.9044	0.9442	0.8860	0.5667
2	0.9188	0.9399	0.8646	0.5564
3	0.9766	0.9047	0.8063	0.5371
4	0.9276	0.8842	0.8782	0.5338
5	0.9311	0.9310	0.8612	0.5675

of a river illustrates the cross-section of the channel and its linear measurements downstream. Further, it also represents the present and the past geomorphic activities. After plotting the long profiles of each watershed,  $R^2$  values of linear, exponential, logarithmic and power curves were obtained. Stream length gradient index (SL) represents intensity of erosional and depositional activities.

Eight basin-scale parameters have been considered for cluster analysis of each watershed (Table 2a, b). Each stream segment was compared with the neighbouring segments to determine the degree of similarity using the Euclidean-based dissimilarity method. The diagram shows the hierarchical relationship between the indicators. This was performed using the formula:

$$\left( \sum_{i=0}^n (X_i - Y_i)^2 \right)^{0.5} \quad (\text{Eqn 3; Clubb et al., 2019})$$

Here  $d_R$ : Euclidean-based dissimilarity,  $X_i$ : distance between the segments,  $Y_i$ : difference of the steepness index between the pair of profiles,  $n$ : number of segments, and  $i$ : element in the array. Hierarchical clustering was done using the  $d_R$  values in the SPSS software (version 26 2019) using the Ward's/minimum variance method. A dendrogram is prepared to demonstrate the relation amongst the segments.

## 5.2. Bathymetric and gravity studies

We generated a bathymetry anomaly map by taking the General Bathymetric Chart of the Oceans (GEBCO) bathymetry (Internet ref-1) data and free-air gravity (FAG) data from the International Gravimetric Bureau (Internet ref-2).

The information about tectonic boundaries, gravity extension and trends are commonly analysed by two or more detection edge techniques (e.g., Kumar et al., 2022; Pal et al., 2016). These techniques estimate several gravity parameters commonly known as the first vertical derivative (FVD), the total horizontal derivative (THD) and the tilt derivative ratio (TDR). These parameters provide low and rounded amplitudes for deeper sources as well as high and sharp amplitudes for shallower sources. The FVD reveals zero amplitudes at the edge locations for the vertical source and has been effectively implicated by several investigations (e.g., Ganguli et al., 2019; Horo et al., 2020; Kumar et al., 2022; Pal et al., 2016). The technique improves the responses from the source of shallower boundaries by controlling the regional responses. Subsurface structures especially lineaments can be interpreted efficiently from these parameters (review in Cheunteu Fantah et al., 2022). The FVD gravity anomaly ( $g_z$ ) amplitudes with respect to the elevation height ( $z$ ) are calculated as follows (Evjen, 1936):

$$FVD = \frac{\partial g_z}{\partial z} \quad (\text{Eqn 4})$$

The THD amplitude utilizes the x- and y-directional derivatives combined response and is computed as follows (Miller and Singh,

1994):

$$THD = \sqrt{\left( \frac{\partial g_z}{\partial x} \right)^2 + \left( \frac{\partial g_z}{\partial y} \right)^2} \quad (\text{Eqn 5})$$

The arctan ratio of FVD to THD amplitudes is known as TDR. It varies between  $-\pi/2$  and  $\pi/2$ . The technique provides zero amplitudes at the vertical boundary sources over the source axis. TDR is estimated as follows (Miller and Singh, 1994):

$$TDR = \tan^{-1} \left( \frac{FVD}{THD} \right) \quad (\text{Eqn 6})$$

These kinds of enhancement techniques used first-order derivatives and several combined derivatives of the potential fields. Their results better enhance the anomalies. The techniques are also able to provide linear, circular and rectangular tectonic boundary enhancement at varying depths up to the Moho (Narayan et al., 2017; Kumar et al., 2022).

## 6. Results & analysis

### 6.1. Morphometry

#### 6.1.1. Stream orders and aspect slope direction

The stream ordering map shows that the watersheds 1–3 have fifth-order streams. Watersheds 4 and 5 have fourth-order streams. Watersheds 1–3 developed possibly over heterogeneous rocks (such as charnockites, mafic units, khondalites, supracrustals, migmatites and recent cover). However, watersheds 4 and 5 are under the homogeneous lithology (e.g., migmatites and recent cover).

This study classified the slopes of all the watersheds into five categories. The slope varies from 0 to  $70^\circ$ . The aspect map shows the direction and degree of slope of the terrain. The aspect tool in ArcGIS classifies the aspect direction map as flat, north, northeast, east, southeast, south, southwest, west, northwest and north (Fig. 2).

#### 6.1.2. Linear geomorphic indicators

6.1.2.1. Hypsometric curve (HC). HCs are used to comprehend the geomorphic cycle of the river. Convex HCs have high values of Hypsometric integral (HI). Such HCs represent rivers' youth stage. Convex-concave HC with medium values of HI represents a mature stage of rivers, and a concave HC with low values of HI connotes the rivers' old stage. A convex HC is characterized by less eroded regions. An S-shaped HC indicates moderately eroded, and a concave HC a highly eroded terrain. In this study, HCs were generated for all the watersheds. Watersheds 4 and 5 demonstrate convex HCs indicating that these watersheds are in disequilibrium stage (Farhan et al., 2016) within the eroded regions. Watersheds 1–3 have slightly S-shaped HCs depicting moderate erosion (Fig. 3).

6.1.2.2. Longitudinal profile. A longitudinal profile is a cross-sectional representation of a river course, which plots elevation along the x-axis and downstream distance along the y-axis. It provides an opportunity to interpret the surface history, e.g., erosional activities, watershed evolution and geologic structures (Costigan et al., 2014). Longitudinal profile aids in identifying knick points, river response to the tectonic uplift or subsidence and the variation in climate and lithology (Kirby et al., 2003; Pérez-Peña et al., 2009).

Source to mouth plot is used to represent longitudinal profiles of the five master streams of the watersheds in this study (Fig. 4a–e). Hence longitudinal profile represents a decrease in the elevation with distance. The coefficient of determination ( $R^2$ ) is obtained

**Table 2**

a. Details of equations of considered spatial and linear parameters for the study								
Sl. No.	Formula for basin scale indicators	Equations & meaning of symbols	Explanations			References		
1.	Hypsometric integral (HI)	$\frac{(\text{Ele}_{\text{avg}} - \text{Ele}_{\text{min}})}{(\text{Ele}_{\text{max}} - \text{Ele}_{\text{min}})}$ Ele <sub>avg</sub> : Average of elevation Ele <sub>min</sub> : Minimum elevation Ele <sub>max</sub> : Maximum elevation	The hypsometric integral is a dimensionless number that allows different sub-basins to be compared regardless of the scale. Hypsometric Integral indicates both tectonic activeness and lithological control. The rate of relief uplift is positively correlated with the hypsometric integral. HI value varies between 0 and 1 and a value nearer to 1 indicate a tectonically very active basin, 0.5 HI value is an indicator of equilibrium (mature) state and a value nearer to 0 indicates tectonically less active basin. Pike and Wilson (1971) mathematically derived the simpler form of hypsometric integral and shown proved that it is a valid approximation of actual hypsometric integral				Strahler (1952), Pike (2000).	
2.	Elongation ratio ( $R_e$ )	$R_e = 1.128 \sqrt{\frac{A}{L_b}}$ A: signifies the area of the basin, L <sub>b</sub> : denotes the length of the basin.	Elongation ratio is influenced by geology and climate. The values vary from 0 to 1 (e.g. Wołosiewicz, 2018). As the landscape evolves, the river basin becomes circular and the value tends to be 1.				Schumm (1956), Wołosiewicz (2018)	
3.	Lemniscate coefficient (k)	$k = \frac{\pi L_b^2}{4A_B}$ Where, A <sub>B</sub> is the area of basin and L <sub>b</sub> is the length of the basin.	Lemniscate coefficient based on expression at basin with Lemniscate curve (i.e. ratio of basin area to its length) in order to determine the shape of the basin. Higher Lemniscate values indicate an elongated basin, which in term denote tectonically very active drainage basin, whereas the low Lemniscate values are associated with less tectonically active basin.				Chorley (1957)	
4.	Asymmetry factor (AF)	$AF = \left( \frac{A_r}{A_t} \right) * 100$ A <sub>r</sub> : area of the basin (km <sup>2</sup> ) to the right of the main channel facing downstream and A <sub>t</sub> : total area (km <sup>2</sup> ) of the basin.	An indicator to measure how much a river basin is tilted due to tectonics. Tectonic activity causes the main stream to change course, sloping away from the basin's midline				Hare and Gardner (1985), Anand and Pradhan (2019)	
5.	Ruggedness number (Hd)	Hd = R*D R = Basin relief D = Drainage density of the basin	Surface unevenness as topographic differentiation is measured.				Horton (1945)	
6.	Form Factor ( $R_f$ )	$R_f = \frac{A_B}{(L_b)^2}$ Here Form ratio ( $R_f$ ), ratio of the basin area (A <sub>B</sub> ) to the square of its length (L <sub>b</sub> )	If the 'R' value of the basin is small then the basin will be more elongated and experience lower peak flows of longer duration while the basin with high 'R' experiences higher peak flows of smaller period.				Horton (1945), Kale et al. (2014)	
7.	Drainage texture (D <sub>t</sub> )	D <sub>t</sub> = Nu/P Nu: Number of streams of a given order. P: Perimeter (km) of the watershed	Drainage texture is influenced by the underlying lithology, infiltration potential, and relief features of the terrain. According to Horton (1945), D <sub>t</sub> is the total number of stream segments along the watershed's margin in all orders. According to various natural characteristics, including climate, precipitation, vegetation, rock/soil type, permeability, undulations, and the stage of watershed development, this is the relative channel spacing on fluidly prepared terrain. Contrarily, T is the result of the addition of D <sub>d</sub> and F. By dividing the drainage density by the present frequency, it is determined. If less than 4, T is classified as a coarse drainage texture. Intermediate drainage structure if it is between 4 and 10; fine drainage structure if it is between 10 and 15; ultrafine drainage structure if it exceeds 15.				Cox (1994)	
8.	Transverse Topographic Symmetry Factor (T)	$T = \frac{Da}{Dd}$ Da: the distance from the drainage basin's midline to the meander belt's midline Dd: the distance from the basin's midline to the basin divide.	T in a perfectly symmetric basin has a value of zero. As asymmetry develops, T likewise rises and eventually reaches a value of one. For various lengths of stream channels, the transverse topographic symmetry factor is computed and reveals the stream's preferred migration direction perpendicular to the drainage axis.				Cox (1994)	
b. Results of calculation of considered unitless parameters for clustering								
Watershed	Elongation Ratio ( $R_e$ )	Form Factor ( $R_f$ )	Ruggedness Number (Hd)	Drainage Texture (D <sub>t</sub> )	Hypsometric Integral (HI)	Asymmetry Factor (AF)	Transverse Topographic Symmetry Factor (T)	Lemniscate Coefficient (K)
1	0.761	0.456	7.300	0.449	0.120	12.057	0.312	1.723
2	0.749	0.441	12.018	0.452	0.084	1.699	0.202	1.780
3	0.638	0.320	25.030	0.380	0.133	6.860	0.573	2.453
4	0.591	0.275	7.731	0.152	0.141	27.193	0.629	2.857
5	0.552	0.239	8.262	0.300	0.162	26.604	0.409	3.283
Class 1	0.552–0.591	0.239–0.275	12.019–25.030	0.386–0.452	0.137–0.162	12.058 –27.193	0.487–0.629	2.858–3.283
Class 2	0.592–0.638	0.276–0.320	8.263–12.018	0.290–0.385	0.111–0.136	6.861–12.057	0.345–0.486	1.781–2.857
Class 3	0.639–0.761	0.321–0.456	7.300–8.262	0.152–0.289	0.084–0.110	1.699–6.860	0.202–0.344	1.723–1.780

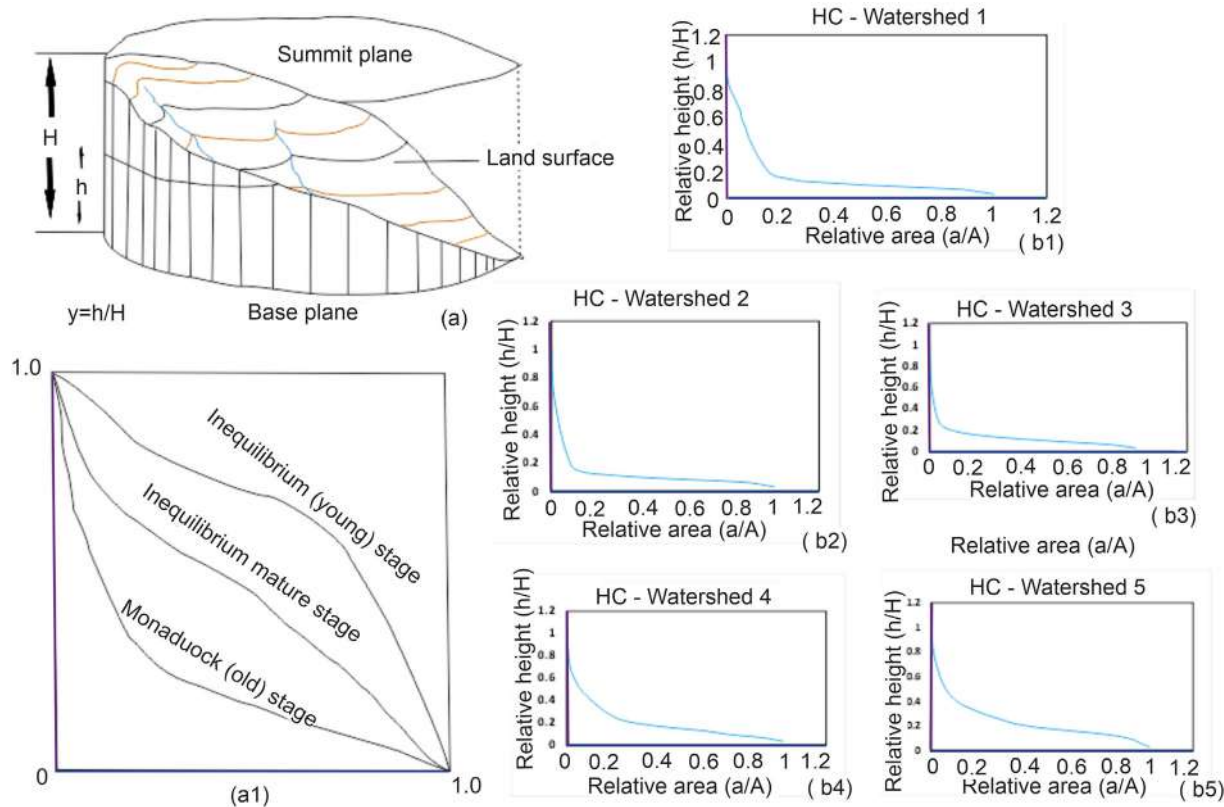


**Fig. 3.** HC- Hypsometric curve. (a) and (a1) Conceptual hypsometric curves indicate young, mature and old stages of rivers. (b1-5) Hypsometric curves of master streams of the watersheds.

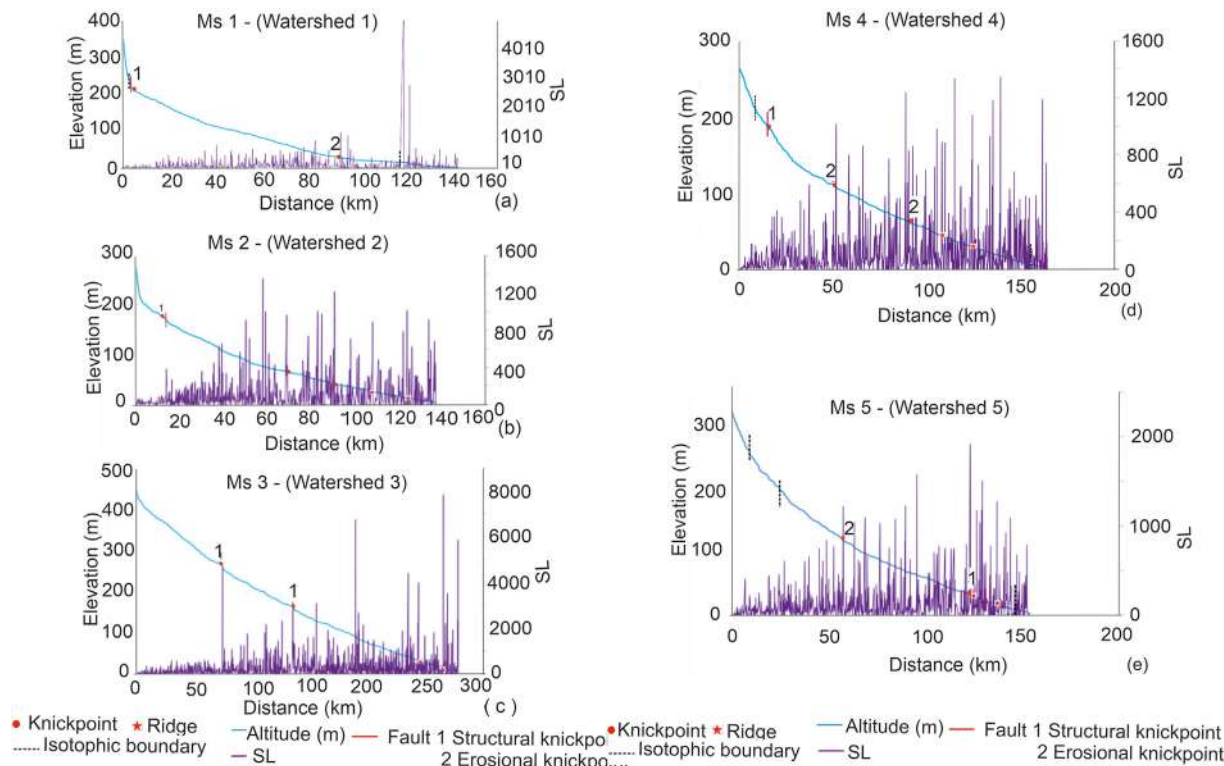


**Fig. 4.** Longitudinal profiles of five master streams (MS) with SL graphs and knickpoints, ridges and isotropic boundaries are marked.

from the graph from which the degree of active tectonics of the rivers and watersheds can be deduced.  $R^2$  values in linear, exponential, logarithmic and power curve fitting of five master streams were calculated (Table 1). Master-streams of watersheds 2–5 show the highest  $R^2$  values in linear curve fitting (0.9188, 0.9766, 0.9276 and 0.9311, respectively); hence, these watersheds may be tectonically very active.

**6.1.2.3. Stream length gradient index (SL).** SL represents the geometry of the longitudinal profile. SL can detect any perturbations in the profile (Troiani et al., 2014). Stream channels affected by geologic systems show anomalies in their profiles and consequently in the SL. SL is the ratio of change in elevation to the change in length of a stream multiplied by total stream length. In this study, only SL variations are plotted along with the longitudinal profile to assess the tectonics of the study area. Watershed 2–5 show more significant variations in SL, in the middle to lower course of the rivers where structural/erosional knick points, faults, ridges etc. can be ascertained (Fig. 4a–e).

#### 6.1.3. Basin-scale parameters

Several techniques have been used on river networks to understand the recent tectonics. These techniques typically consider the homogeneity of the base rock. Geologic terrains can be diverse in terms of variations in uplift rates, rock strength, climate and geomorphic processes (Clubb et al., 2019). Clubb et al. (2019) recommended combining river profiles with similar morphologies so that tectonic, climatic and/or lithologic controls could be identified. By grouping such constraints, clustering may differentiate signal from noise (source signals). This method uses unsupervised classification. Hierarchical clustering of watersheds is done in this study. Based on how closely related the various parameters are to one another, the segments are grouped. The considered morphometric parameters enabled to determine a symmetric proximity matrix between each pair of segments of indicators (Table 3).

Watersheds 2, 4 and 5 come under cluster 1 in the dendrogram where the considered basin scale parameters are rescaled as per the magnitudes. The cluster range is 10–25 (Fig. 5a). Cluster 1 indicates structural control in channel morphology.

## 6.2. Bathymetric & gravity works

#### 6.2.1. Bathymetric studies

We prepared a regional contour map of the selected region (Fig. 1b) in the MATLAB 2017 environment, which covers the region of Gulf of Mannar in the Indian sector. Contour plot shows that the bathymetric depth gradually increases along the north-south trend from the coast to the central region of the gulf (Fig. 1b). It varies from 500 m in the coast to >1800 m depth in the centre (Fig. 1b). More than 1500 m deep Gulf of Mannar lying between India and Sri Lanka is characterized by biannual reversing wind monsoon. To study the circulation of surface and coastal upwelling in waters around Sri Lanka, de Vos et al. (2013) implemented a regional ocean modelling system for the northern ocean of India, which covers the

**Table 3**

Results of calculation of considered parameters for clustering as proximity matrix, in terms of correlation between vectors of values.

Case	1	2	3	4	5
1	1.000	0.498	0.625	0.956	0.963
2	0.498	1.000	0.986	0.223	0.249
3	0.625	0.986	1.000	0.370	0.394
4	0.956	0.223	0.370	1.000	0.999
5	0.963	0.249	0.394	0.999	1.000

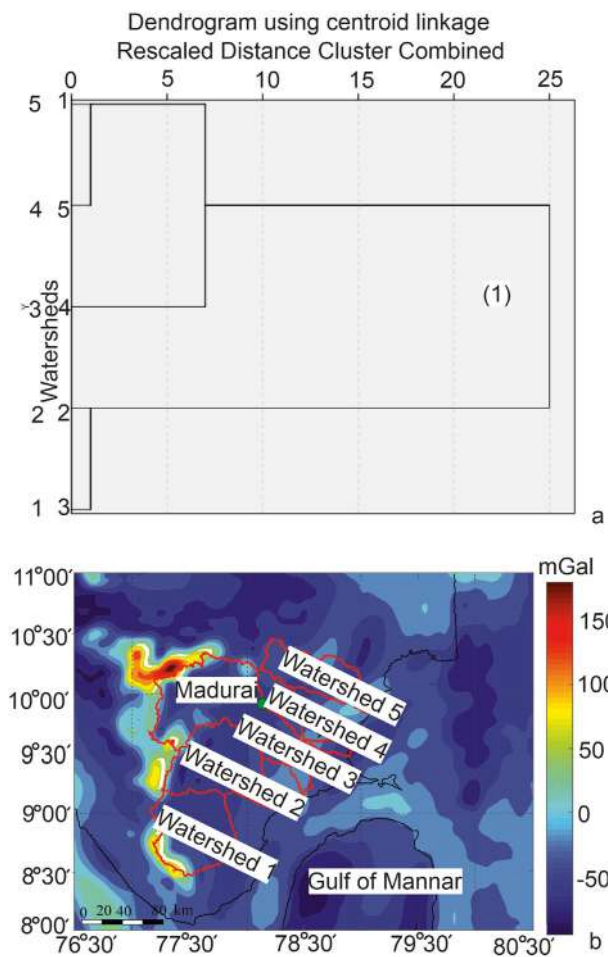


**Fig. 5.** (a) Dendrogram with a single cluster developed. (b) Free air gravity anomaly contour plot in the selected region.

southern part of the Indian mainland and as well as Sri Lanka. The results showed that the region faces seasonal differences in cooling and heating of the continental landmass and ocean (de Vos et al., 2013).

#### 6.2.2. Gravity studies

The free-air gravity (FAG) data is used and a map is prepared for land part from the EGM2008 data (Fig. 5b). Fig. 5b shows that the gravity contour map has a very sharp gradient of gravity anomalies. The regional area of continental shelf demonstrates a relatively positive gravity anomaly, which includes partially watersheds 1 and 3. The anomaly slowly becomes negative towards the basin area. These gravity values, which are high in the continental shelf region, ranges from ~−30 to 160 mGal. The basinal area shows low values ranging from ~−30 to −80 mGal. These low values occur because of increased sediment thickness near the foot of the slope (such as Dar et al. (2015)). Alternately, presence of hydrocarbon reserve can be the other reason. However, this needs confirmation from more geoscientific inputs. Kumar et al. (2009a, 2009b) used Bouguer anomaly gravity measurement from this region that covered all the watersheds of this study. The low gravity may be caused by combined effects of exposed geologic formations and deeper Moho because of isostatic compensation (Singh et al., 2003, 2006).

Another striking feature in the gravity map is the correspondence between coastline and the gravity contours. Gravity

observations along the coast indicate a low-density thick continental plate and a denser thin oceanic plate (Kumar et al., 2009a,b). Krishna et al. (2002) noticed a quasi/wide continental shelf in the eastern Arabian sea and the adjoining Indian west coast (extension around  $63^{\circ}30'E$  to  $78^{\circ}20'E$  and  $5^{\circ}N$  to  $23.30^{\circ}N$ ), which however refutes this suggestion. Thus, the western Indian coast's high gravity is attributed to deep faults, which upwarped the Moho, and/or placed ultrabasic high-density rocks at shallower depths (Brahmam, 1993; Subrahmanyam and Verma, 1986). Moderate variation of gravity covers low central and a high coastal gravity, and characterizes the region of south-central part (watersheds 1–3). Gravity contours follow the Mannar basin's structural grains in the oceanic region (Kumar et al., 2009a,b).

## 7. Discussions

### 7.1. Morphometry

A tectonic map consisting of faults, lineaments and ridges was prepared using data from the previously published articles related to the tectonic of the study area (Fig. 2). Several NW-SE trending faults and lineaments control/deflect the drainages. Most of the rivers in the study area are fault-controlled, exhibiting dextral-slip (as in Ramasamy, 2006; Praseeda et al., 2015).

As per longitudinal profile and their  $R^2$  values, watersheds 2–5 are tectonically highly active since they show high to moderate  $R^2$  values (0.9766, 0.9276 and 0.9311). The SL graphs of watersheds 2 and 3 vary widely, whereas the disparity is moderate for

watersheds 5 and 6. These differences are due to the tectonic disturbances in the terrain. The Asymmetry Factor of watershed 4 shows the highest value ( $AF = 27.193$ ), and watershed 2 has the lowest value ( $AF = 1.699$ ). This indicates that watershed 4 is highly asymmetric and may be tilted tectonically. The low elongation values indicate zones of active uplift and youth stages of rivers. Watersheds 1 and 2 show concave curves representing a highly eroded and old stage of the river. Watershed 1 consists of a perennial river exhibiting 'z'-shaped deviated stream. In terms of the  $R_e$  magnitudes, watersheds 4 and 5 are highly elongated (0.591 and 0.552, respectively), and watersheds 1–3 (0.761, 0.749 and 0.638, respectively) are elongated moderately. The high elongation values are only seen in active uplift and youth stage of the river.

From the dendrogram, it is evident that watersheds 4 and 5 are more active tectonically. Several N-S extensional faults, NE-SW sinistral and NW-SE dextral faults and lineaments (Ramasamy, 2006) have impacted the river dynamics within these watersheds. Tectonic adjustments related to faults developed knick points. The river channel of watershed 4 shows a notable change in the direction of flow, possibly due to the basin's tectonic inheritance and transient landscape. The river persists in its linear and narrow basin. Deflection of the river channel due to lateral tilting of the watershed due to tectonic activities can be seen in both the watersheds 4 and 5.

The spatial drainage patterns connote the structural signatures in the south-eastern part of the watersheds 4 and 5 that fall inside the Rammad-Palk Sub-basin. Near the confluence, basement faults (Fig. 3), neotectonic faults and major and minor lineaments control

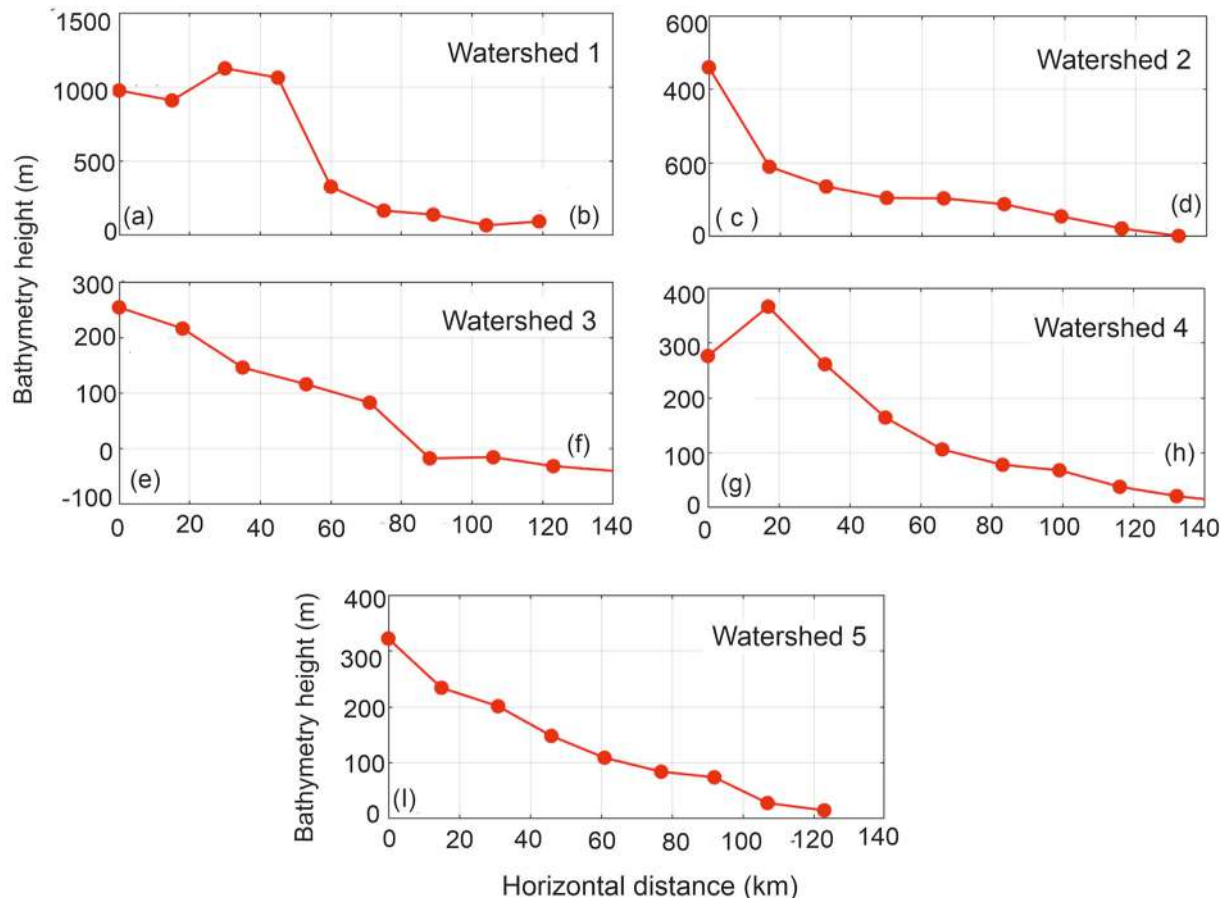


**Fig. 6.** Red lines: bathymetry height variations along the selected watersheds.

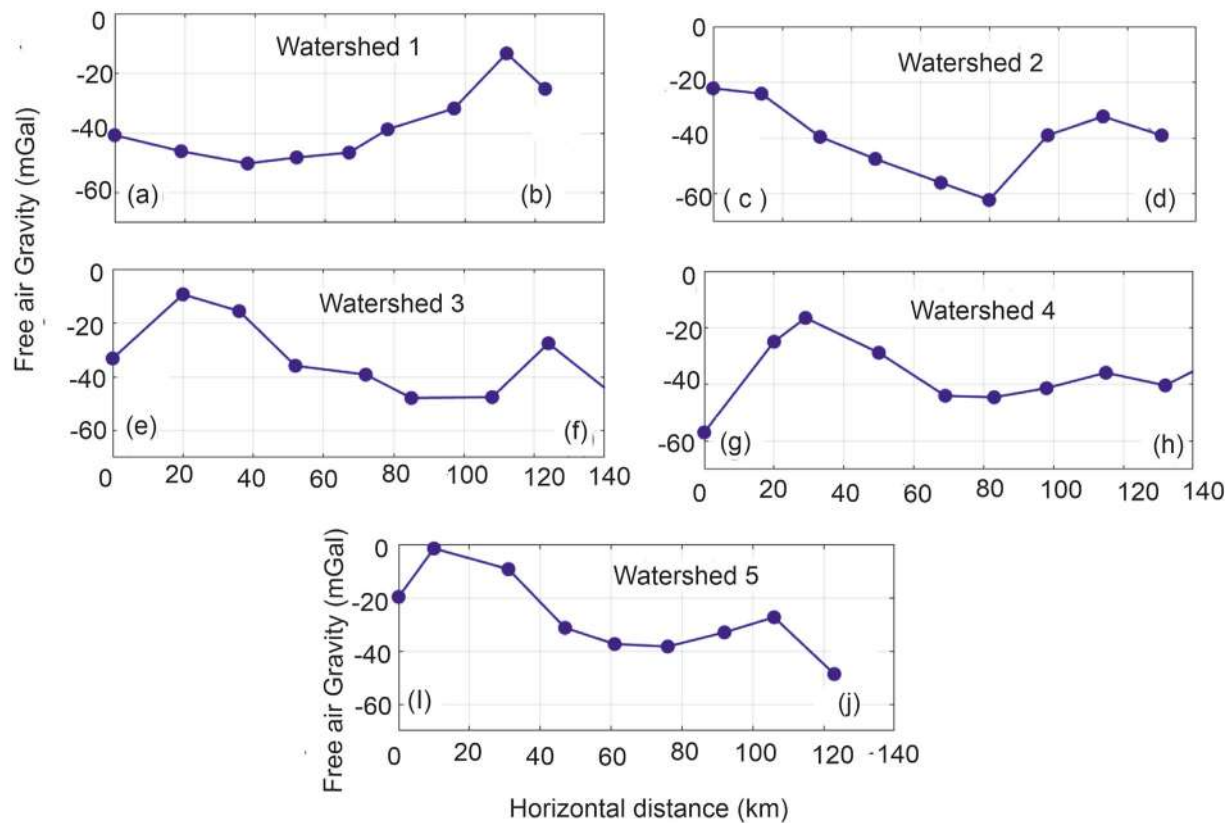


**Fig. 7.** Blue lines: gravity variations along the selected watersheds.

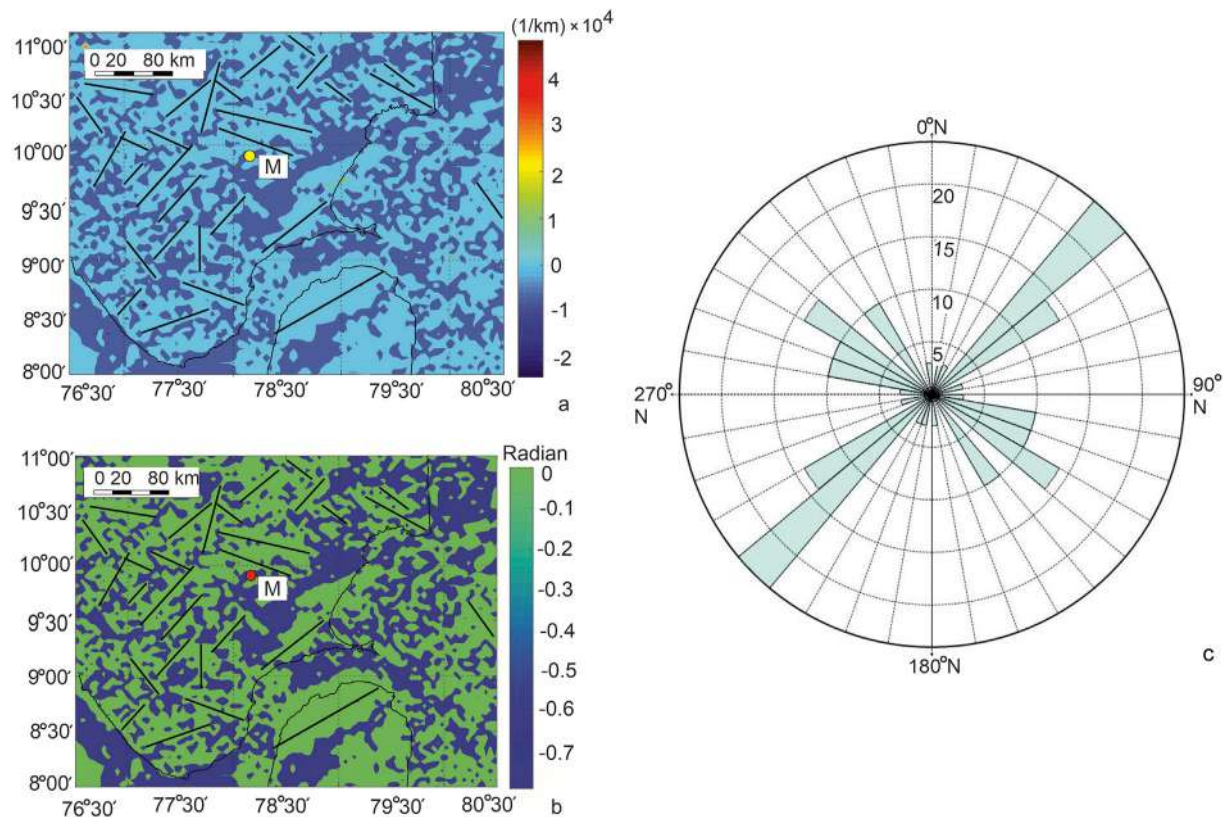


**Fig. 8.** (a) The delineated lineaments estimated by the FVD with edge extension (black lines). Colour bar: FVD amplitude of gravity anomaly in  $104 \text{ km}^{-1}$ . (b) Black lines: lineaments deduced from TDR. Colour bar: TDR amplitude in radian. (c) Rose diagram of lineaments (Software: [Rose.Net](#). Version: 0.10.0.0. Year: 2012).

the channels' flow towards SE. The elevated topography related to the unnamed basement faults and NW-SE shear zones possibly acted as a water divide of watersheds 4 and 5. Middle to lower part of the watersheds 4 and 5 lie between the Mannargudi ridge and the Tanjavur depression. Neotectonic faults e.g., Amaradakki Fault, Manamelkudi-Tondi Fault, Vaigai River Fault, subsurface faults with bedding joints and several lineaments trend NW-SE and NE-SW.

Watershed 1 is moderately to less active. Interestingly, Achankovil Shear Zone that passes through this watershed was active in the Neoproterozoic (Plavsa et al., 2014). This fault might be much less active at present. This can explain the near-circular shape of the watershed 1.  $AF = 12.058 - 27.193$  for the watersheds 4 and 5 indicates that these two basins come under Class 1. The range of  $R_e$  (0.591 and 0.552, respectively), HI (0.141 and 0.162, respectively) and k (3.283 and 2.858–3.283, respectively) of watershed 4 and 5 are under Class 1 and indicate that they are presently active tectonically.

## 7.2. Bathymetry & gravity models

The bathymetric elevation and depth plots for all the selected watersheds along the horizontal distance from their starting point (eastern border of Indian continent) is shown in Fig. 6. The extension and variation of shelf along watersheds can be deciphered from this figure. The shelf widths the watersheds 1 and 5 are ~120 km, while it is > 120 km for watersheds 2–4. Generally, the elevation trend of shelf width reduces from the eastern coast to the Indian continent.

The free air gravity vs. the horizontal distance plots for all the selected watersheds from their starting points at the eastern margin of Indian continent is shown in Fig. 7. The figure shows that the gravity anomaly along the selected watersheds is categorized by superimposed numerous lows and highs. Apparently, the positive correlation between surface elevation (Fig. 6) and free air gravity magnitudes (Fig. 7) can be seen for watersheds 2–5. Elevation variation for different watersheds in Fig. 6 differs. The average gravity variation for each watershed is -60 to 0 mGal. This indicates the state of conjecture and overcompensation because of a shortfall of mass effect at subcrustal depth. In watersheds 1–4, relatively appeared high gravity (~10 mGal) dominates the band of high-density quartzite and iron formation and is apparently caused by the near surface geology (Kumar et al., 2009a,b).

We first estimated the FVD and then the TDR to delineate the edges as lineaments with their higher accuracy of spatial occurrence and trends (Fig. 8a–c). The delineated lineaments locate the edge extensions (black lines) of the relevant sources that can be related to the basement faults, blocks fractures and shear zones. The lineament diagrams are identified from edge enhanced maps and respective plots with their strikes. These lineament plots reveal the trend of the major structural features to be along NW-SE and NE-SW.

The Gulf of Mannar experienced two-stage rifting/continental breakup associated with separation of Gondwanaland during the Mesozoic era. This resulted in tectonic disturbances in the basin. It produced N-S extensional and NE-SW sinistral faults, NW-SE dextral faults and lineaments (Ramasamy, 2006). These NW and NE-trending faults and lineaments control the course of streams and deflect the drainages. The river networks are affected by tectonic activities such as faulting and rifting. Most of the rivers in the study area are controlled by dextral strike-slip faults.

## 8. Conclusions

The northeastern part of the study area (watersheds 4 and 5) is more tectonically active than the southeastern portion (watersheds

1–3). Middle to lower part of the watershed 4 lies between Mannargudi ridge. Several NW-SE trending faults (Vaigai River Fault, Amaradakki Fault and Manamelkudi-Tondi Fault) and a NE-trending one (e.g., Rajamatam-Davipattinapm Fault) (and a single hot spring) pass through (/are close to) these watersheds indicating that these faults might be active at present or in the recent past. Any wells drilled in these two watersheds must take care of the issue of their stability. On the other hand, the Achankovil Shear Zone passing through watershed 1 seems to be presently (almost) inactive. The bathymetry results showed that the depth gradually increases along the north-south trend from the coast towards the central region of the Gulf. It varies from the depth of 500 m in the coast to >1800 m depth in the center. The bathymetry and the gravity anomalies bear positive correlation between surface elevation and free air gravity magnitudes for all the watersheds. However, the degree of this correlation varies for each watershed. The lineament plots using the FVD and TDR techniques reveal that the trend of the major structural features (basement faults, blocks fractures and shear zones) trend NE-SW and NW-SE. Some of these lineaments match with the trend of the surface lineaments compiled.

## CRediT authorship contribution statement

**Kutubuddin Ansari:** Writing – original draft, Investigation. **Mery Biswas:** Writing – original draft, Investigation. **Adrija Raha:** Writing – original draft, Investigation. **M.L. Shilpasree:** Writing – original draft, Investigation. **Soumyajit Mukherjee:** Writing – review & editing, Supervision, Funding acquisition.

## Declaration of competing interest

The authors declare that there is no conflict of interest regarding the publication of this article.

## References

- Aiken, S.J., Brierley, G.J., 2013. Analysis of longitudinal profiles along the eastern margin of the Qinghai-Tibetan Plateau. *J. Mt. Sci.* 10, 643–657.
- Ali, J.R., Aitchison, J.C., 2008. Gondwana to Asia: plate tectonics, paleogeography and the biological connectivity of the Indian sub-continent from the Middle Jurassic through latest Eocene (166–35 Ma). *Earth Sci. Rev.* 88, 145–166.
- Anand, A.K., Pradhan, S.P., 2019. Assessment of active tectonics from geomorphic indices and morphometric parameters in part of Ganga basin. *J. Mt. Sci.* 16, 1943–1961.
- Biswas, M., Gogoi, M.P., Mondal, B., Sivasankar, T., Mukherjee, S., Dasgupta, S., 2022a. Geomorphic assessment of active tectonics in Jaisalmer basin (western Rajasthan, India). *Geocarto Int.* 37, 12382–12413.
- Biswas, M., Puniya, M.K., Gogoi, M.P., Dasgupta, S., Mukherjee, S., Kar, N.R., 2022b. Morphotectonic analysis of petroliferous Barmer rift basin (Rajasthan, India). *Earth System Science* 131, 140.
- Brahmam, N.K., 1993. Gravity in relation to crustal structure, paleosutures and seismicity of southern India. *Mem. Geol. Soc. India* 25, 165–201.
- Brandt, S., Raith, M.M., Schenk, V., Sengupta, P., Srikanthappa, C., Gerdes, A., 2014. Crustal evolution of the Southern Granulite Terrane, south India: new geochronological and geochemical data for felsic orthogneisses and granites. *Precambr. Res.* 246, 91–122.
- Chari, M.N., Sahu, J.N., Banerjee, B., Zutshi, P.L., Chandra, K., 1995. Evolution of the Cauvery basin, India from subsidence modelling. *Mar. Petrol. Geol.* 12, 667–675.
- Chatterjee, S., Goswami, A., Scotese, C.R., 2013. The longest voyage: tectonic, magmatic, and paleoclimatic evolution of the Indian plate during its northward flight from Gondwana to Asia. *Gondwana Res.* 23, 238–267.
- Cheunteu Fantah, C.A., Mezoue, C.A., Mouzong, M.P., Tokam Kamga, A.P., Nouayou, R., Nguuya, S., 2022. Mapping of major tectonic lineaments across Cameroon using potential field data. *Earth Planets Space* 74, 1–19.
- Chorley, R.J., 1957. Illustrating the laws of morphometry. *Geol. Mag.* 94, 140–150.
- Clark, C., Collins, A.S., Timms, N.E., Kinny, P.D., Chetty, T.R.K., Santosh, M., 2009. SHRIMP U-Pb age constraints on magmatism and high-grade metamorphism in the Salem Block, southern India. *Gondwana Res.* 16, 27–36.
- Clubb, F.J., Bookhagen, B., Rheinwald, A., 2019. Clustering river profiles to classify geomorphic domains. *J. Geophys. Res.: Earth Surf.* <https://doi.org/10.1029/2019jf005025>.
- Collins, A.S., Pisarevsky, S.A., 2005. Amalgamating eastern Gondwana: the evolution

- of the Circum-Indian Orogens. *Earth Sci. Rev.* 71, 229–270.
- Costigan, K.H., Daniels, M.D., Perkin, J.S., Gido, K.B., 2014. Longitudinal variability in hydraulic geometry and substrate characteristics of a Great Plains sand-bed river. *Geomorphology* 210, 48–58.
- Cox, R.T., 1994. Analysis of drainage-basin symmetry as a rapid technique to identify areas of possible Quaternary tilt-block tectonics: an example from the Mississippi Embayment. *Geol. Soc. Am. Bull.* 106, 571–581.
- Dar, A.M., Lasitha, S., Rammiyin, K., 2015. A gravity and bathymetric study in the south east continental margin of India. *J. Remote Sens. GIS* 4 (3).
- Das, S.K., Phanishekhar, N., Mahadevan, R., 2008. Understanding of volcanic intrusives and hydrocarbon Habitat through integrated study in Gulf of Mannar offshore, Cauvery Basin. In: 7th International Conference and Exposition on Petroleum Geophysics, Society of Petroleum Geophysicists, pp. 14–16.
- Dasgupta, S., Pande, P., Ganguly, D., Iqbal, Z., Sanyal, K., Venkatraman, N.V., Dasgupta, S., Sural, B., Harandranath, L., Mazumder, K., Sanyal, S., Roy, A., Das, L.K., Mishra, P.S., Gupta, S., 2000. Seismotectonic atlas of India and its environs. In: Narula, P.L., Acharya, S.K., Banerjee, J. (Eds.), Geological Survey of India. Director General Geological Survey of India, p. 80.
- Dasgupta, S., Biswas, M., Mukherjee, S., Chatterjee, R., 2022. Structural evolution and sediment depositional system along the transform margin–Palar–Pennar basin, Indian east coast. *J. Petrol. Sci. Engineer* 211, 110155.
- Dasgupta, S., 2019. Implication of transfer zones in rift fault propagation: example from Cauvery basin, Indian east coast. In: Mukherjee, S. (Ed.), *Structural Geology and Tectonics: Indian Context*. Springer Geology, Cham, pp. 313–326.
- de Vos, A., Pattiaratchi, C.B., Wijeratne, E.M.S., 2013. Surface circulation and upwelling patterns around Sri Lanka. *Biogeosci. Discuss.* 10, 14953–14998.
- Desa, M., Ramana, M.V., Ramprasad, T., 2006. Seafloor spreading magnetic anomalies south off Sri Lanka. *Mar. Geol.* 229, 227–240.
- Dmitrieva, E., Jackson, C.A.L., Huuse, M., Kane, I.A., 2018. Regional distribution and controls on the development of post-rift turbidite systems: insights from the Paleocene of the eastern North Viking Graben, offshore Norway. In: Bowman, M., Levell, B. (Eds.), *Petroleum Geology Conference Series*, 8, pp. 147–170.
- Dwivedi, A.K., 2016. Petroleum exploration in India—a perspective and endeavours. *Proc. Indian Natl. Sci. Acad.* 82, 881–903.
- Evjen, H.M., 1936. The place of the vertical gradient in gravitational interpretations. *Geophysics* 1, 127–136.
- Farhan, Y., Mousa, R., Dagarah, A., Shtaya, D., 2016. Regional hypsometric analysis of the Jordan Rift drainage basins (Jordan) using Geographic Information System. *Open J. Geol.* 6, 1312–1343.
- Fraefel, M., 2008. *Geomorphic Response to Neotonic Activity in the Jura Mountains and the Southern Upper Rhine Graben (Thesis)*. Swiss Federal Institute of Forest, Snow and Landscape Research WSL, pp. 1–163.
- Galushkin, Y.I., Dubinin, E.P., 2020. Thermal history and extension of the lithosphere in the Mannar basin and realization its hydrocarbon potential, offshore Sri Lanka. *Mar. Petrol. Geol.* 119, 104477.
- Ganguli, S.S., Singh, S., Das, N., Maurya, D., Pal, S.K., Rama Rao, J.V., 2019. Gravity and magnetic survey in southwestern part of Cuddapah Basin, India and its implication for shallow crustal architecture and mineralization. *J. Geol. Soc. India* 93, 419–430.
- Ghosh, J.G., de Wit, M.J., Zartman, R.E., 2004. Age and tectonic evolution of Neo-proterozoic ductile shear zones in the Southern Granulite Terrain of India, with implications for Gondwana studies. *Tectonics* 23, TC3006.
- Gopalankrishnan, K., 2003. An over view of southern Granulite Terrain, India – constraints in reconstructions of precambrian assembly of Gondwanaland. *Mem. Geol. Soc. India* 50, 47–48.
- Hare, P.W., Gardner, T.W., 1985. Geomorphic indicators of vertical neotectonism along converging plate margins, Nicoya Peninsula, Costa Rica. *Tectonic Geomorphology* 4, 75–104.
- Harinarayana, T., Naganjaneyulu, K., Manoj, C., Patro, B.P.K., Kareemunnisa Begum, S., Murthy, D.N., Rao, Madhusudana, Kumaraswamy, V.T.C., Virupakshi, G., 2003. Magnetotelluric investigations along Kuppam-Palani geotransect, south India- 2-D modelling results. In: Singh, A.P., Mishra, D.C., Vijaya, Kumar, V., Rao, M.B.S.V. (Eds.), *Tectonics of Southern Granulite Terrain: Kuppam-Palani Geotransect*. Memoir Geological Society of India, pp. 107–124.
- Herath, P., Gunatilek, J., Weerasinghe, D., 2017. Mohorivitic discontinuity beneath Mannar Basin: a failed rift. *J. Geol. Soc. Sri Lanka* 18, 77–87.
- Horo, D., Pal, S.K., Singh, S., Srivastava, S., 2020. Combined self-potential, electrical resistivity tomography and induced polarisation for mapping of gold prospective zones over a part of Babaikundi-Birgaon Axis, North Singhbum Mobile Belt, India. *Explor. Geophys.* 51, 507–522.
- Horton, R.E., 1945. Erosional development of streams and their drainage basins; hydrophysical approach to quantitative morphology. *Geol. Soc. Am. Bull.* 56, Internet ref-1: URL: [http://www.gebco.net/data\\_and\\_products](http://www.gebco.net/data_and_products) (Accessed on 12-July-2023).
- Internet ref-2: URL: <https://bgi.obs-mip.fr/data-products/outils/egm2008-anomaly-maps-visualization/> (Accessed on 13-July-2023).
- Kale, V.S., Sengupta, S., Achyuthan, H., Jaiswal, K.M., 2014. Tectonic controls upon Kaveri River drainage, cratonic Peninsular India: inferences from longitudinal profiles, morphotectonic indices, hanging valleys and fluvial records. *Geomorphology* 227, 153–165.
- Kirby, E., Whipple, K.X., Tang, W., Chen, Z., 2003. Distribution of active rock uplift along the eastern margin of the Tibetan Plateau: inferences from bedrock channel longitudinal profiles. *J. Geophys. Res. Solid Earth* 108, <https://doi.org/10.1029/2001JB000861>.
- Krishna, M.R., Verma, R.K., Purushotham, A.K., 2002. Lithospheric structure below the eastern Arabian Sea and adjoining west coast of India based on integrated analysis of gravity and seismic data. *Mar. Geophys. Res.* 23, 25–42.
- Kularathna, E.K.C.W., Pitawala, H.M.T.G.A., Senaratne, A., Ratnayake, A.S., 2020. Play distribution and the hydrocarbon potential of the Mannar Basin, Sri Lanka. *J. Pet. Explor. Prod. Technol.* 10, 2225–2243.
- Kumar, N., Singh, A.P., Rao, M.P., Chandrasekhar, D.V., Singh, B., 2009a. Gravity signatures, derived crustal structure and tectonics of Achankovil Shear Zone, southern India. *Gondwana Res.* 16, 45–55.
- Kumar, N., Singh, A.P., Rao, M.P., Chandrasekhar, D.V., Singh, B., 2009b. Gravity signatures, derived crustal structure and tectonics of Achankovil Shear Zone, southern India. *Gondwana Res.* 16, 45–55.
- Kumar, U., Narayan, S., Pal, S.K., 2022. Structural and tectonic interpretation of EGM2008 gravity data around the Laccadive ridge in the Western Indian Ocean: an implication to continental crust. *Geocarto Int.* 37, 3179–3198.
- Lal, N.K., Siawal, A., Kaul, A.K., 2009. Evolution of east coast of India - a plate tectonic reconstruction. *J. Geol. Soc. India* 73, 249–260.
- Mahadevan, T.M., 2003. Geological evolution of South Indian Shield- constrains on modelling. *Mem. Geol. Soc. India* 50, 25–46.
- Mathew, M.J., Menier, D., Siddiqui, N., Ramkumar, M., Santosh, M., Kumar, S., Hassaan, M., 2016. Drainage basin and topographic analysis of a tropical landscape: insights into surface and tectonic processes in northern Borneo. *J. Asian Earth Sci.* 124, 14–27.
- Miller, H.G., Singh, V., 1994. Potential field tilt—a new concept for location of potential field sources. *J. Appl. Geophys.* 32, 213–217.
- Mishra, C.K., Dewangan, P., Mukhopadhyay, R., Banerjee, D., 2021. Velocity modeling and attribute analysis to understand the gas hydrates and free gas system in the Mannar Basin, India. *J. Nat. Gas Sci. Eng.* 92, 104007.
- Mohan, M.R., Satyanarayanan, M., Santosh, M., Sylvester, P.J., Tubrett, M., Lam, R., 2013. Neoarchean suprasubduction zone arc magmatism in southern India: geochemistry, zircon U-Pb geochronology and Hf isotopes of the Sittampudi Anorthosite Complex. *Gondwana Res.* 23, 539–557.
- Narasaiha, R., 2017. India's energy Security: potentials of BIMSTEC in perspective. *ISDA J.* 27, 21–45.
- Narayan, S., Sahoo, S.D., Pal, S.K., Kumar, U., Pathak, V.K., Majumdar, T.J., Chouhan, A., 2017. Delineation of structural features over a part of the Bay of Bengal using total and balanced horizontal derivative techniques. *Geocarto Int.* 32, 351–366.
- Pal, S.K., Majumdar, T.J., Pathak, V.K., Narayan, S., Kumar, U., Goswami, O.P., 2016. Utilization of high-resolution EGM2008 gravity data for geological exploration over the Singhbhum-Orissa Craton, India. *Geocarto Int.* 31, 783–802.
- Pérez-Peña, J.V., Azanón, J.M., Booth-Rea, G., Azor, A., Delgado, J., 2009. Differentiating geology and tectonics using a spatial autocorrelation technique for the hypsometric integral. *J. Geophys. Res.: Earth Surf.* 114, 1–15.
- Pike, R.J., Wilson, S.E., 1971. Elevation-relief ratio, hypsometric integral, and geomorphic area-altitude analysis. *Geol. Soc. Am. Bull.* 82, 1079–1084.
- Pike, R., 2000. Geomorphometry – diversity in quantitative surface analysis. *Prog. Phys.* 24, 1–20.
- Piyadasa, H.T.N.I., 2014. *Marine Environment Protection from Offshore Oil and Gas: Activities in Sri Lanka (Thesis)*. World Maritime University, pp. 1–94.
- Plavsa, D., Collins, A.S., Payne, J.L., Foden, J.D., Clark, C., Santosh, M., 2014. Detrital zircons in basement metasedimentary protoliths unveil the origins of southern India. *Geol. Soc. Am. Bull.* 126, 791–811.
- Prabhakar, K.N., Zutshi, P.L., 1993. Evolution of southern part of Indian east coast basins. *J. Geol. Soc. India* 41, 215–230.
- Praseeda, E., John, B., Srinivasan, C., Singh, Y., Divyalakshmi, K.S., Samui, P., 2015. The normal fault system, Southern India: implication to neotectonics. *J. Geol. Soc. India* 86, 391–398.
- Praveen, M.N., Santosh, M., Yang, Q.Y., Zhang, Z.C., Huang, H., Singanenjam, S., Sajinkumar, K.S., 2013. Zircon U-Pb geochronology and Hf isotope of felsic volcanics from Attappadi, southern India: implications for Neoarchean convergent margin tectonics. *Gondwana Res.* 26, 907–924.
- Premarathne, U., Ranaweera, L.V., 2021. Continental flood basalt magmatism contemporaneous with Deccan traps in the Mannar basin, offshore Sri Lanka. *Isl. Arc* 30, e12409.
- Premarathne, D.M.U.A.K., Suzukil, N., Ratnayake, N.P., Kularathne, E.K.C.W., 2013. A petroleum system in the gulf of Mannar Basin, offshore Sri Lanka. In: Proceedings to 29th Technical Sessions of Geological Society of Sri Lanka.
- Premarathne, D.M.U.A.K., 2015a. Basin and petroleum system modeling of the northern Mannar Basin, offshore Sri Lanka (Doctoral Dissertation). In: Division of Earth and Planetary System Science, Department of Natural History Sciences. Graduate School of Science, Hokkaido University, p. 6.
- Premarathne, D.M.U.A.K., 2015b. Basin and Petroleum System Modeling of the Northern Mannar Basin, Offshore Sri Lanka (Ph.D. thesis). Hokkaido University. <https://doi.org/10.14943/doctoral.k12052>.
- Radhakrishna, B.P., 1993. Neogene uplift and geomorphic rejuvenation of the Indian Peninsula. *Curr. Sci.* 64, 787–793.
- Ramana, M.V., Nair, R.R., Sarma, K., Ramprasad, T., Krishna, K.S., Subrahmanyam, V., D'Cru, M., Subrahmanyam, C., Paul, J., Subrahmanyam, A.S., Chandra Sekhar, D.V., 1994a. Mesozoic anomalies in the Bay of Bengal. *Earth Planet Sci. Lett.* 121, 469–475.
- Ramana, M.V., Nair, R.R., Sarma, K.V.L.N.S., Ramprasad, T., Krishna, K.S., Subrahmanyam, V., 1994b. Mesozoic anomalies in the Bay of Bengal. *Earth Planet Sci. Lett.* 121, 469–475.
- Ramana, M.V., Ramprasad, T., Desa, M., 2001. Seafloor spreading magnetic anomalies in the Enderby basin, East Antarctica. *Earth Planet Sci. Lett.* 191, 241–255.

- Ramasamy, S.M., 2006. Remote sensing and active tectonics of South India. *Int. J. Rem. Sens.* 27, 4397–4431.
- Ratheeesh-Kumar, R.T., Dharmapriya, P.L., Windley, B.F., Xiao, W.J., Jeevan, U., 2020. The tectonic “Umbilical Cord” Linking India and Sri Lanka and the Tale of their failed rift. *J. Geophys. Res. Solid Earth* 125, e2019JB018225.
- Ratnayake, N.P., Puswewala, U.G.A., Chaminda, S.P., Ekanayaka, E.M.T.M., Jayawardene, A.M.N., 2014. Evaluation of the potential of sea sand as an alternative to river sand for concrete production in Sri Lanka. *Journal of Geological Society of Sri Lanka* 16, 109–117.
- Reddy, P.R., Rajendra Prasad, B., Vijaya Rao, V., Sain, K., Prasad Rao, P., Reddy, P.K., 2003. Deep seismic reflection and refraction/wide angle reflection studies along Kuppam-Palani transect in the southern Granulite terrain of India. *Mem. Geol. Soc. India* 50, 79–106.
- Resmi, M.R., Achyuthan, H., Babeesh, C., 2021. Holocene evolution of the Palar river, Southern India: tracking history of migration, provenance, weathering and tectonics. *Quat. Int.* 575, 358–374.
- Resmi, M.R., Achyuthan, H., Chauhan, G., Deopa, H., 2022. Late Quaternary landscape evolution of Peninsular India: a review based on fluvial archives. In: Mishra, S.P., Sethi, K.C. (Eds.), *Holocene Climate Change and Environment*. Elsivier, pp. 441–456.
- Różycka, M., Migoń, P., 2021. Morphometric properties of river basins as indicators of relative tectonic activity – problems of data handling and interpretation. *Geomorphology* 389, 107807.
- Samuel, V.O., Santosh, M., Liu, S., Wang, W., Sajeev, K., 2014. Neoarchean continental growth through arc magmatism in the Nilgiri Block, southern India. *Precambr. Res.* 245, 146–173.
- Santosh, M., Shaji, E., Tsunogae, T., Mohan, M.R., Satyanarayanan, M., Horie, K., 2013. Suprasubduction zone ophiolite from Agali hill: petrology, zircon SHRIMP U–Pb geochronology, geochemistry and implications for Neoarchean plate tectonics in southern India. *Precambr. Res.* 231, 301–324.
- Satyanarayana, G.V., Singh, R., Mukhopadhyay, R., Singh, M.K., Mohan, K.G., Baraik, S., 2016. Interpretation of marine magnetic and bathymetry data off Kanyakumari-Vembar, gulf of Mannar, Tamil Nadu coast, Bay of Bengal. *J. Geophys.* 37, 55–64.
- Schumm, S.A., 1956. Evolution of drainage systems and slopes in Badlands at Perthamboy, New Jersey. *Bull. Geol. Soc. Am.* 67, 597–646.
- Singh, A., Rao, G.S., 2021. Crustal structure and subsidence history of the Mannar basin through potential field modelling and back stripping analysis: implications on basin evolution and hydrocarbon exploration. *J. Petrol. Sci. Eng.* 206, 109000.
- Singh, A.P., Mishra, D.C., Kumar, V.V., Rao, M.B.S.V., 2003. Gravity-magnetic signatures and crustal architecture along Kuppam-Palani Geotransect, South India. *Memoirs-Geological Society of India* 139–164.
- Shaji, E., Santosh, M., He, X.F., Fan, H.R., Dev, S.D., Yang, K.F., Thangal, M.K., Pradeepkumar, A.P., 2014. Convergent margin processes during Archean–Proterozoic transition in southern India: geochemistry and zircon U–Pb geochronology of gold-bearing amphibolites, associated metagabbros, and TTG gneisses from Nilambur. *Precambr. Res.* 250, 68–96.
- Singh, A.P., Kumar, N., Singh, B., 2006. Nature of the crust along Kuppam–Palani geotransect (South India) from gravity studies: implications for precambrian continental collision and delamination. *Gondwana Res.* 10, 41–47.
- Sivakumar, V., 2016. Geological, geomorphological and lineament mapping through remote sensing and GIS techniques, in parts of Madurai, Ramanathapuram and Tiruchirappalli districts of Tamil Nadu. *Int. J. Geomatics Geosci.* 6, 1669–1675.
- Štěpánčíková, P., Stemberk, J., Vilímek, V., Košťák, B., 2008. Neotectonic development of drainage networks in the East Sudeten Mountains and monitoring of recent fault displacements (Czech Republic). *Geomorphology* 102, 68–80.
- Storey, M., Mahoney, J.J., Saunders, A.D., Duncan, R.A., Kelley, S.P., Coffin, M.F., 1995. Timing of hot spot-related volcanism and the breakup of Madagascar and India. *Science* 267, 852–855.
- Strahler, A.N., 1952. Hypsometric (area-altitude) analysis of erosional topography. *Geol. Soc. Am. Bull.* 63, 1117–1142.
- Subrahmanyam, C., Verma, R.K., 1986. Gravity field, structure and tectonics of the Eastern Ghats. *Tectonophysics* 126, 95–212.
- Thanikachalam, M., Ramachandran, S., 2002. Management of coral reefs in Gulf of Mannar using Remote sensing and GIS techniques-with reference to coastal geomorphology and land use. *Map Asia*. In: *Asian Conference on GIS, Aerial Photography and Remote Sensing*. Bangkok, pp. 7–9.
- Troiani, F., Galve, J.P., Piacentini, D., Della Setta, M., Guerrero, J., 2014. Spatial analysis of stream length-gradient (SL) index for detecting hillslope processes: a case of the Gállego River headwaters (Central Pyrenees, Spain). *Geomorphology* 214, 183–197.
- Twinkle, D., Rao, G.S., Radhakrishna, M., Murthy, K.S.R., 2016. Crustal structure and rift tectonics across the Cauvery–Palar basin, Eastern Continental Margin of India based on seismic and potential field modelling. *J. Earth Syst. Sci.* 125, 329–342. Geomorphic domains.
- Vasudevan, K., Ramana, L.V., Nagasudha, V., Borthakur, A., Das, S.K., 2008. Petroleum system and play types of Synrift sequences, Ramanand Subbasin, Cauvery Basin. In: *7<sup>th</sup> International Conference & Exposition, Society of Petroleum Geophysicists*.
- Wolosiewicz, B., 2018. The influence of the deep-seated geological structures on the landscape morphology of the Dunajec River catchment area, Central Carpathians, Poland and Slovakia. *Contemp. Trends Geosci.* 1 (7), 1–11.
- Zhang, M.H., Qiao, J.H., Zhao, G.X., Lan, X.Y., 2019. Regional gravity survey and application in oil and gas exploration in China. *China Geology* 2, 382–390.